C. R. Physique 16 (2015) 97–104

Contents lists available at ScienceDirect

Comptes Rendus Physique

www.sciencedirect.com

Granular physics / Physique des milieux granulaires

The structure of powder snow avalanches

Structure des avalanches en aérosol

Betty Sovilla [a,*], Jim N. McElwaine [b], Michel Y. Louge [c]

[a] *WSL Institute for Snow and Avalanche Research SLF, Flüelastrasse 11, 7260 Davos Dorf, Switzerland*
[b] *Department of Earth Sciences, Durham University, Durham DH1 3LE, United Kingdom*
[c] *Sibley School of Mechanical and Aerospace Engineering, Cornell University, Ithaca, NY 14853, United States*

ARTICLE INFO

Article history:
Available online 6 December 2014

Keywords:
Snow entrainment
Avalanche impact pressure
Avalanche velocity
Avalanche density
Mixed avalanches
Powder snow avalanches

Mots-clés :
Avalanches mixtes
Avalanches en aérosol

ABSTRACT

Powder snow avalanches (PSAs) can be hundreds of metres high and descend at astonishing speeds. This review paints a composite picture of PSAs from data acquired at the Vallée de la Sionne test site in Switzerland, including time-histories of snow cover thickness from buried RADAR and, at several elevations on a pylon, impact pressures from load cells, air pressure, particle velocity from optical sensors, and cloud density and particle cluster size from capacitance probes. PSAs feature distinct flow regions with stratification in mean density. At the head, highly fluctuating impact pressures weaken with elevation, while vertical velocity profiles evolve rapidly along the flow, suggesting that surface snow layers of light, cold, cohesionless snow erupt into a turbulent, inhomogeneous, recirculating frontal cloud region. For hundreds of metres behind the head, cloud stratification sharpens with the deposition of suspended cloud particles, while a denser basal flow of increasing thickness forms as deeper, warmer and heavier parts of the weakened snow cover are entrained. Toward the tail, vertical velocity profiles are more uniform, impact pressures become lower and steadier as the flow becomes thinner, and snow pack entrainment is negligible.

RÉSUMÉ

Les avalanches en aérosol peuvent atteindre plusieurs centaines de mètres de hauteur et dévaler à des vitesses étonnantes. Cette revue peint une image générique de ces avalanches à partir de données obtenues sur le site de la vallée de la Sionne, en Suisse. Ces données incluent l'épaisseur du manteau neigeux en fonction du temps, observée par un radar enfoui et, à plusieurs hauteurs sur un pylône, des pressions d'impact provenant de cellules de charge, des mesures de pression de l'air, des vitesses de particules par l'intermédiaire de capteurs optiques et, enfin, la densité de l'aérosol et la taille de ses amas, par une sonde à capacité. Les avalanches en aérosol comprennent des zones distinctes, avec stratification de la densité moyenne. À leur front, les pressions d'impact fluctuent, mais s'affaiblissent avec la hauteur, alors que les profils verticaux de vitesse évoluent rapidement le long de l'écoulement. Ceci suggère que des couches de neige légère, froide et sans cohésion font éruption en créant une région frontale turbulente, hétérogène et recirculante. Sur des centaines de mètres derrière le front, la stratification de l'aérosol s'accroît avec la

* Corresponding author.
E-mail addresses: sovilla@slf.ch (B. Sovilla), james.mcelwaine@durham.ac.uk (J.N. McElwaine), MYL3@cornell.edu (M.Y. Louge).

http://dx.doi.org/10.1016/j.crhy.2014.11.005
1631-0705/

déposition de particules suspendues. Un écoulement de surface à épaisseur croissante s'établit alors, tandis que des éléments plus chauds et plus profonds du manteau neigeux sont entraînés. Vers la queue de l'avalanche, les profils verticaux s'uniformisent, la pression d'impact et ses fluctuations diminuent, alors que l'écoulement s'affine et que l'érosion du manteau neigeux devient négligeable.

1. Introduction

Powder snow avalanches (PSAs) are destructive flows as high as 200 m descending at frontal speeds of up to 100 $\mathrm{m\,s^{-1}}$. Dry snow PSAs typically develop a dilute frontal region feeding an energetic turbulent suspension, and visibly feature a slow sedimenting cloud trailing far behind. They typically originate from a dense flow, which remains hidden and travels behind the front, thus evoking the term "mixed" PSAs. In the literature [1–4], there is not currently a unified view of the structure and behaviour of PSAs, mainly because of a lack of experimental information.

In this review, we combine recent measurements obtained from several events at the Vallée de la Sionne (VdlS) test site to paint a synoptic picture of a mixed PSA. We devote sections to insights that each instrument provides, and we synthesize a generic description illustrated by cartoons of the flow.

2. Field data

The limited optical depth of PSAs and their destructive power severely constrain measurement techniques. While video imaging can delineate their outline [5], peering inside the avalanche requires microwave apparatus [6–8] or robust instruments attached to an invasive pylon [9,10]. There are few facilities in the world that can record snow pack entrainment [11], air pressure [12,13], cloud height and speed [5,14], impact pressure [15–18] and cloud density [19,20]. However, all these measurements can be performed at the VdlS simultaneously. Because every avalanche may follow a different path, it is difficult to place instruments at an optimum location or to compare signals from separate events. Nonetheless, it is possible to paint a synoptic picture of mixed PSAs from available data.

Instruments mentioned in this review include Frequency-Modulated Continuous-Wave (FMCW) Radar buried in the ground (snow cover thickness) [6,11], and probes deployed on the oval-shaped, 20 m-tall steel pylon shown in Fig. 1, including load cells (impact pressure) [21,22], optical fiber sensors (velocity) [9,23], a Pitot probe (air pressure) at 10 m elevation over hard ground [12], and capacitance probes (snow density and cluster size) [24]. The pylon also carried flow depth sensors between 0.25 m and 7.5 m.

Figs. 3 and 5 to 7 feature cartoons drawn with exaggerated elevation to illustrate flow and snow cover structure. They are matched with actual signals, converted from time to distance using measurements of local mean flow velocity [9]. The cartoons delineate five numbered regions with distinct behavior, illustrated with composite data from different PSAs.

3. Experimental data

3.1. Air pressure

Conventional sensors measuring air speed, such as hot-wire or ultrasonic anemometers, are either too fragile or unreliable in PSAs. However, a Pitot probe is strong enough to generate useful data [12,26,27]. The VdlS pylon supported a probe with one transducer averaging pressure over several holes. It recorded $p_a = p - p_0 - (13/64)\rho u^2$, where p and u are local air static pressure and flow speed, ρ is mean suspension density, and p_0 is background atmospheric pressure.

Outside a PSA, air is subject to a potential flow, except in a thin layer above the snow cover and in a relatively narrow wake. There, as the inset in Fig. 2 illustrates, the flow may be approximately described by a dipole, yielding a static pressure in excess of the ambient in frontal region A. Further back and to the side, static pressure is below ambient in region B. Eventually, far from the front but close to the top or side of the PSA, pressure fluctuates in the turbulent wake [25,28,29].

If the PSA passes straight over the pylon (bottom Fig. 2), the signal in region A reaches a maximum as its nose hits the sensor. Pressure then drops linearly as the pylon is swept by region 2, sinking deeply below ambient and betraying the presence of large-scale recirculation within the head; further back, the signal then turns turbulent.

PSA size and speed can be estimated from measurements in regions A and B, i.e. before the avalanche hits the pylon. Inside the PSA, pressure and its fluctuations reveal the existence of coherent structures, such as large-scale vortices, and intense turbulence. In the head, mean velocity can be higher than the front velocity u_f [25,30,31], suggesting that forces on a structure may rise to levels greater than what a calculation based on u_f alone might predict.

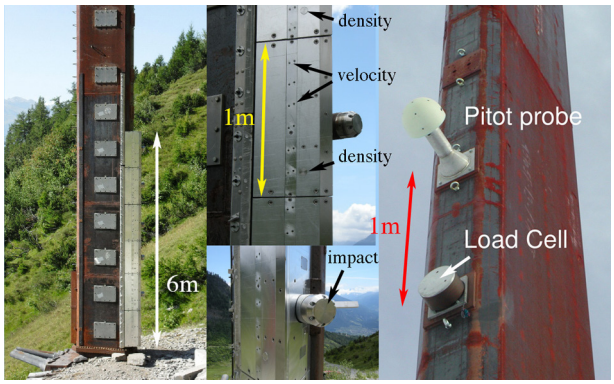

Fig. 1. (Color online.) The 20 m-high VdlS instrumented pylon. Left: overview. Centre: optical sensors, capacitance probes and close-up of an impact load cell. Right: air pressure Pitot probe and a high frequency load cell. Vertical scale is shown.

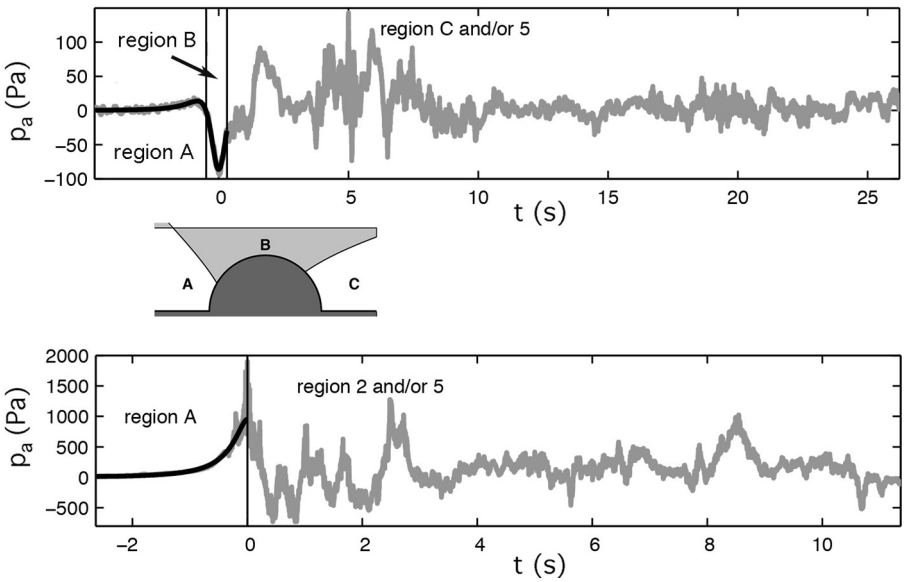

Fig. 2. Upper panel: Air pressure p_a (Pa) measured in and around a PSA on January 19, 2004 mostly passing to the side of the pylon vs time t (s). The dark line shows the dipole fit and $t = 0$ corresponds to the front of the avalanche being level with the pylon. It is unclear when the sensor entered the avalanche. Lower panel: Air pressure measurement from another PSA on January 19, 2004 passing nearly straight over the pylon. $t = 0$ corresponds to its arrival at the pylon. The inset illustrates the three pressure regions for the flow over a semi-circle [25]. Region A has pressure above ambient; region B has pressure below (i.e. a negative "gauge pressure"); the flow is separated in region C. The line between regions A and B is exact, whereas the line between B and C is figurative since the separation point can change.

3.2. Snow entrainment

Snow pack entrainment is crucial to the dynamics of PSAs. Without it, air mixed at their outer interface would rapidly dilute the suspension, quenching turbulence intensity, decelerating the flow, and sedimenting particles. At the VdlS, PSAs pick up from one to twelve times their initial release mass, or a factor of four on average. The bulk of this erosion occurs just behind the front with entrainment rates as high as 350 $\mathrm{kg\,m^{-2}\,s^{-1}}$ [11]. Snow may be directly ejected into the powder cloud through large mean pore pressure gradients induced by the flow within the underlying porous snow cover [12,28,34], or entrained at the surface by turbulent fluctuations.

Fig. 3 shows signals from one of six FMCW Radar [6] installed at the VdlS. Although interpretation remains qualitative, the corresponding time-history offers insight on entrainment location and rate [11]. At the front (region 1), the PSA produces rapid lifting of the snow cover that is more reminiscent of an eruption than a gradual erosion. The weakened snow cover then gets further entrained by subsequent denser slides as far as ~ 100 m behind the front (region 3) [8].

Although no instruments were positioned in the VdlS starting zone, videos reveal that PSAs typically begin as a dense flow after release across a wide slab. As the resulting slide descends, it grows, accelerates and gradually incorporates more material. When it reaches a sufficient speed, particles are launched on high ballistic trajectories while air turbulent eddies scour further material from the surface, thus turning the slide into a mixed PSA. At this point, the dilute front (region 1) usually travels ahead of a denser slide.

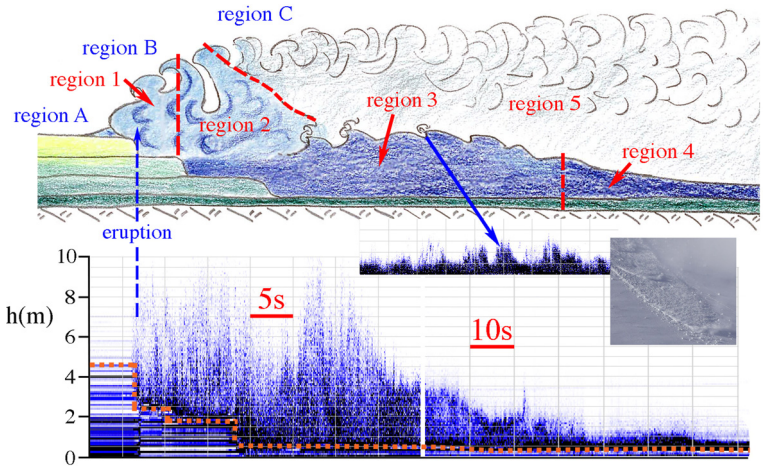

Fig. 3. (Color online.) Upper panel: cartoon schematic of a mixed PSA entraining a generic layered snow cover, with numbered and lettered regions mentioned in the text. Lower panel: composite FMCW RADAR signal time-history of a PSA on December 27, 1999, converted to elevation h in m. The time scale in the early signal is magnified. Horizontal lines in the signal on the left reveal stratigraphic variations of the snow cover before passage of the front, with heavier color indicating denser or wetter layers. The dashed orange line marks the estimated elevation of the remaining stable snowpack. An inset shows a FMCW signal from a similar PSA suggesting the formation of roll-waves in region 3, of a kind pictured on the right. The avalanche entrains large parts of the snow cover in the head region by step-wise, abrupt snow eruptions. Between these eruptions, scraping of snow from the sliding surface (basal erosion) is small and cannot be discerned in the FMCW signal.

Fig. 4. (Color online.) Left panel: mixed PSA artificially released at the VdlS test site. Right panel: deposited granules formed in a dense flow after entrainment of snow typically at −1 to 0 °C [32,33]. A glove shows scale.

PSAs typically involve dry, cohesionless snow. However, they may also coexist with wet snow avalanches if the pack changes from dry to wet along their path. Generally, variability of snow entrainment into PSAs arises from an inherent diversity in stratigraphy of the snow pack (density, temperature, water content) [35].

Because snow sintering depends on temperature and load [36], the considerable forces that a PSA induces within the snow cover can determine whether the entrained material forms granules or maintains its original fine-grained morphology. Similarly, because freshly-deposited surface snow is cold, its ability to sinter is limited, and it may be brought into suspension more easily. In contrast, warmer snow near the ground at −1 to 0 °C might rapidly sinter into larger granules [32] (Fig. 4). In general, a cold and light snow cover typically fluidises [29,34], while warmer, wetter or more cohesive snow may form a denser core behind the front [11].

PSAs dwindle once they can no longer entrain fresh snow. Without it, their suspension density drops as they engulf air at the interface. Turbulence intensity decays and particles settle, sharpening the density stratification. This decline occurs mostly in a widening runout zone, or upslope if the erodible snow supply disappears.

3.3. *Density and its fluctuations*

Fig. 5 shows instantaneous snow density recorded with capacitance instruments attached to the pylon. With proper calibration for the VdlS basin [24], these probes detect how much material resides in their measurement volume ~ 1 cm^3. Because snow is not distributed homogeneously and because their response is not linear with density, signal interpretation is not straightforward. However, exploiting their relatively fast 7.5 kHz bandwidth, one may inspect signal fluctuations and

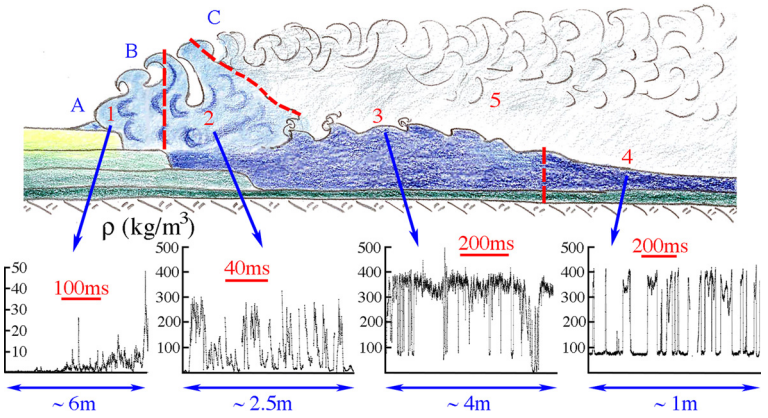

Fig. 5. (Color online.) Measurements of density ρ (kg m^{-3}) in a relatively small PSA on December 6, 2010 with a capacitance probe at 2.7 m elevation above hard ground. Regions, see Fig. 3. The apparent baseline ~ 50 kg m^{-3} of the right signal from region 4 may be due to persistent snow accumulation on the probe face. Distances estimated from local speed and time scales are shown in blue and red, respectively.

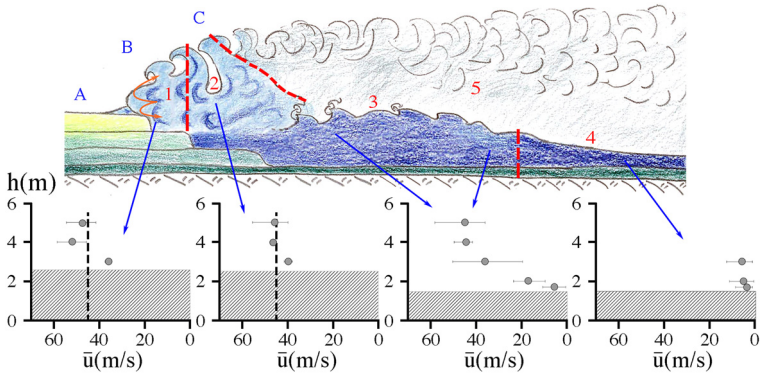

Fig. 6. (Color online.) Typical profiles of mean velocity $\bar{u}$ (m s^{-1}) vs elevation h (m) from cross-correlating optical probe signals as regions 1 to 4 of the PSA on March 3, 2006 traverse the pylon. Vertical dashed lines indicate the estimated avalanche front velocity u_f. Cross-hatching represents depth of the snow pack.

discern whether these are produced by a homogeneous suspension, a particle cluster, or an aggregate. For example, denser aggregates create a relatively tall peak of duration combining their size and speed.

As Fig. 5 illustrates, the mean density increases from regions 1 to 3. At the front (region 1), it is typically $\lesssim 10$ kg m^{-3}, consistent with a dilute suspension of fine-grained snow and theoretical predictions [28]. In clouds with larger mean density, region 1 occasionally experiences short bursts of higher density, perhaps produced by suspended remnants of the snow pack fracturing process. Behind the relatively dilute front, region 2 has higher average density and wider fluctuations. There, turbulence occurs on an increasing scale [37], and likely incorporates particle clusters of higher local concentration [10, 38]. In region 3, density oscillates around a higher average, which is typical of denser slides [24]. Finally, in region 4, the capacitance probe may experience intermittent peaks produced by well formed granules of various sizes flowing by the sensor.

3.4. Velocity profiles

Velocity profiles, velocity fluctuations and strain rates are inferred by cross-correlating optical backscattering signals [19, 39,40]. On the VdlS pylon, sensors with 20 kHz bandwidth are located from the base of the mast up to a height of 6 m with a vertical spacing of 125 mm. Fig. 6 refers to an older configuration with sensors installed at 2, 3, 4 and 5 m above ground. Meanwhile, frontal speed is independently measured by videogrammetry [5,41] or radar [8] located in the bunker.

Fig. 6 shows measurements in a small powder avalanche [9,23]. The highest speeds are found in region 1. There, the velocity near the base is lower than the front speed u_f (marked by a vertical dashed line), and the velocity gradient reverses direction toward higher elevations. The resulting strain rate implies a flow recirculation along the air–cloud interface (clockwise in Fig. 6) and in the opposite direction near the base. Within experimental errors, the measurements also suggest that the peak streamwise velocity in region 1 may exceed the frontal speed. This is consistent with air pressure measurements in Section 3.1, which implied the presence of large vortices. The resulting high speeds may also contribute to material eruption mentioned in Section 3.2.

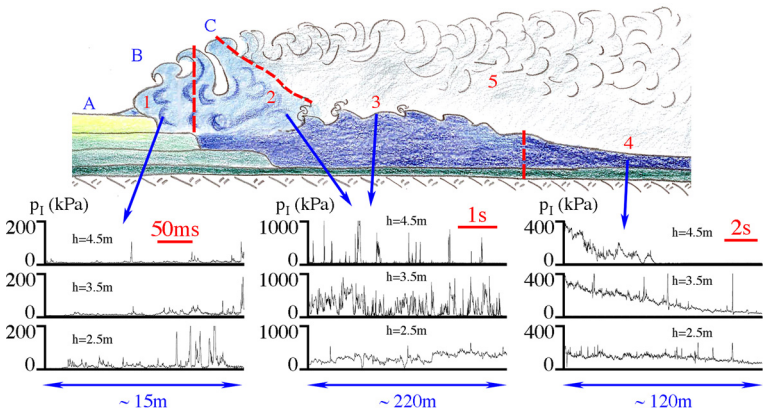

Fig. 7. (Color online.) Typical impact pressures p_I (kPa) in the PSA of Fig. 6 from three load cells positioned at 2.5 m, 3.5 m, and 4.5 m, from bottom to top. Note the different scales: impact pressures are lower in region 1, rise in region 2, and gradually decrease in region 4. Time and distances evaluated as in Fig. 5.

Table 1
Typical parameters of a large PSA at VdlS. (Ranges may be wider for all possible PSAs). u/u_f are estimates of instantaneous downslope velocity relative to the front velocity, as suggested by the magnitude of static pressure fluctuations in Fig. 2, and by mean velocities shown in Fig. 6. Regions A, B and C surround the PSA and are devoid of snow. Air density is represented by 1 $kg\,m^{-3}$.

	Regions	A	B	C	1	2	3	4	5
	Units	Laminar overpressure	Laminar underpressure	Turbulent wake	Dilute front	Energetic suspension	Dense core	Dense tail	Powder cloud
density	$kg\,m^{-3}$	1	1	1	1–30	1–300	250–400	350–500	1–2
u/u_f	·	0–1	1–2	0–1	0–3	0.5–2	0.5	0.2	0.1
p_a	kPa	0–2	−2–0	±2	0–2	0–1	±0.1	±0.1	0–0.5
p_I	kPa	0	0	0	1–100	50–1000	50–400	50–400	0

In region 2, the vertical velocity profile becomes more uniform and is everywhere lower than the front speed. In region 3, velocities high on the mast remain as large as in region 2, but are considerably smaller below, suggesting the presence of a relatively thick (1–3 m) highly sheared dense flow. Finally, speed drops substantially towards the tail (region 4) and the flow behaves as a slowing granular material with smaller shear rate.

3.5. Impact pressure

Piezoelectric load cells of 10 cm diameter are installed on the uphill face of the pylon to record impact pressure every metre from 0.5 m to 5.5 m above hard ground (Fig. 1) [21,22]. Fig. 7 shows signals from a relatively small PSA. The peak pressures here are two to three orders of magnitude larger than the air pressure measurements (Section 3.1) reflecting the much larger density of snow compared to air. In region 1, impact pressure is low and typical of a dilute stratified flow [9]. It consists of impulses lasting ∼ 10 ms, which correspond to the collision of individual blocks of snow (for example a 0.1 m block moving at 10 $m\,s^{-1}$ produces a signal of ∼ 10 ms). The duration and intensity increases toward the base of the flow. In regions 2 and 3, the bursts become more intense but gradually coalesce into a steadier signal toward the base, which is characteristic of a layered, energetic flow [9]. Finally, the signal becomes steadier toward the end of region 3, and its magnitude gradually decreases as this dense flow slows down in region 4.

4. Overview

Figs. 2–3 and 5–7 present composite cartoons of distinct regions in a generic, fully developed, mixed PSA. In regions A, B and C, clear ambient air initially at rest is pushed aside by the incoming PSA. At the front (region 1), flow-induced pore pressure gradients and surface shear stresses directly entrain snow from the porous snow pack. Turbulent mixing keeps the snow in suspension, but is counteracted by particle sedimentation. The balance between turbulence, sedimentation and air entrainment at the upper surface determines the strength of the density stratification [42,43].

Region 2 features a heterogeneous and energetic suspension of snow particles. It is either fed from region 1 or by the erupting snow pack, and it possibly supports the presence of a few large clusters or aggregates. Below, the weakened snow cover is mobilized as a denser region 3 about 100 m behind the front, rapidly sliding near the ground, but typically unable to catch up with the front, as it is significantly slowed by basal drag. On occasion, the FMCW signal in region 3 [44] exhibits oscillations resembling roll waves, which Hopfinger [1] postulated may be associated with inception of the powder cloud.

The tail of the denser avalanche of region 3 then gradually slows down as region 4. As dense sheared granular flows, regions 3 and 4 are likely where aggregates detected by capacitance instruments form (Fig. 5).

There are few measurements in region 5 beside videogrammetry [45]. However, this region likely consists of a nearly-arrested sedimenting suspension cloud produced by the decaying turbulence from region 2 and growing by further air entrainment at the interface [46,47]. Unlike regions 1 and 2, because this cloud is no longer supplied with material from the snow cover, its behavior has greater kinship with lock-exchange gravity currents [48–51].

The most dangerous parts of the flow are regions 2 and 3 [9,21], where impact pressures can reach sufficient levels to destroy wood and brick structures (12–24 kPa and 25–45 kPa, respectively), level mature forests ($\sim$100 kPa), or displace large rocks ($>$200 kPa). The more dilute region 1 also packs enough kinetic energy to damage tall objects such as tree tops or utility poles [52], break windows (2–4 kPa), or weaken doors, walls and roofs (3–6 kPa).

Because traditional gravity currents possess high Reynolds numbers, they are barely affected by basal drag, and thus they can propagate large distances over flat surfaces, and even climb uphill. Their dynamics are determined by an ability to keep snow in suspension while converting potential to kinetic energy [50]. They can only conserve or lose overall weight (called "buoyancy" in the literature). In contrast, PSAs dramatically increase their overall weight through rapid particle entrainment, thus giving them the rather different behaviour of an "eruption current" [29].

5. Outlook and future directions

Direct observations in PSAs have become more common in recent years, but remain limited and difficult to achieve. Point measurements like those at the pylon are useful where the flow varies slowly, but their interpretation becomes more challenging if the PSA evolves more rapidly. Occasionally, PSAs die near the pylon, revealing mechanisms during the deposition phase. Generally, data on the initial phases of avalanche motion and the formation of the powder cloud are lacking. Although information presented here begins to construct a picture of entrainment and mixing, new observations of air pressure, mixture density and air velocity will lead to a better understanding of PSAs, from which further models can be tested.

Acknowledgements

We are grateful to Thierry Faug and Kouichi Nishimura for their insightful comments and suggestions.

References

[1] E. Hopfinger, Snow avalanche motion and related phenomena, Annu. Rev. Fluid Mech. 15 (1983) 47–76.
[2] C. Ancey, Snow avalanches, in: N. Balmforth, A. Provenzale (Eds.), Geomorphological Fluid Mechanics, in: Lect. Notes Phys., vol. 582, Springer, Berlin, Heidelberg, 2001, pp. 319–338.
[3] D. Issler, Experimental information on the dynamics of dry-snow avalanches, in: K. Hutter, N. Kirchner (Eds.), Dynamic Response of Granular and Porous Materials Under Large and Catastrophic Deformations, in: Lect. Notes Appl. Comput. Mech., vol. 11, Springer, Berlin, Germany, 2003, pp. 109–160.
[4] E. Meiburg, J.N. McElwaine, B. Kneller, Turbidity currents and powder snow avalanches, in: H. Fernando (Ed.), Handbook of Environmental Fluid Dynamics, vol. 1, Taylor & Francis, 2012, pp. 557–573.
[5] J. Vallet, U. Gruber, F. Dufour, Photogrammetric avalanche volume measurements at Vallée de la Sionne, Switzerland, Ann. Glaciol. 32 (2001) 141–146.
[6] H. Gubler, M. Hiller, The use of microwave FMCW radar in snow and avalanche research, Cold Reg. Sci. Technol. 9 (1984) 109–119.
[7] L. Rammer, M. Kern, U. Gruber, F. Tiefenbacher, Comparison of avalanche-velocity measurements by means of pulsed Doppler radar, continuous wave radar and optical methods, Cold Reg. Sci. Technol. 50 (1–3) (2007) 35–54, http://dx.doi.org/10.1016/j.coldregions.2007.03.014.
[8] N.M. Vriend, J.N. McElwaine, B. Sovilla, C.J. Keylock, M. Ash, P.V. Brennan, High-resolution radar measurements of snow avalanches, Geophys. Res. Lett. 40 (2013) 727–731.
[9] B. Sovilla, M. Schaer, M. Kern, P. Bartelt, Impact pressures and flow regimes in dense snow avalanches observed at the Vallée de la Sionne test site, J. Geophys. Res. 113 (2008) F01010, http://dx.doi.org/10.1029/2006JF000688.
[10] S.S. Grigorian, N.A. Urumbiev, I.V. Nekrasov, Data of geological studies, Academy of Sciences of the USSR Section of Glaciology of the Soviet Geophysical Committee and Institute of Geography 44 (1982) 87–94 (in Russian).
[11] B. Sovilla, P. Burlando, P. Bartelt, Field experiments and numerical modeling of mass entrainment in snow avalanches, J. Geophys. Res. 111 (2006) F03007, http://dx.doi.org/10.1029/2005JF000391.
[12] J.N. McElwaine, B. Turnbull, Air pressure data from the Vallée de la Sionne avalanches of 2004, J. Geophys. Res. 110 (2005) F03010, http://dx.doi.org/10.1029/2004JF000237.
[13] K. Nishimura, Y. Ito, Velocity distribution in snow avalanches, J. Geophys. Res. 102 (B12) (1997) 27297–27303, http://dx.doi.org/10.1029/97JB02120.
[14] K. Nishimura, N. Maeno, F. Sandersen, K. Kristensen, H. Norem, K. Lied, Observations of the dynamic structure of snow avalanches, Ann. Glaciol. 18 (1993) 313–316.
[15] D.M. McClung, P.A. Schaerer, Characteristics of flowing snow and avalanche impact pressures, Ann. Glaciol. 6 (1985) 9–14.
[16] P. Gauer, D. Issler, K. Lied, K. Kristensen, H. Iwe, E. Lied, L. Rammer, H. Schreiber, On full-scale avalanche measurements at the Ryggfonn test site, Cold Reg. Sci. Technol. 49 (1) (2007) 39–53.
[17] H. Shimizu, T. Huzioka, E. Akitaya, H. Narita, M. Nakagawa, K. Kawada, A study on high-speed avalanches in the Kurobe canyon, Japan, J. Glaciol. 26 (94) (1980) 141–151.
[18] K. Nishimura, H. Narita, N. Maeno, K. Kawada, The internal structure of powder-snow avalanches, Ann. Glaciol. 13 (1989) 207–210.
[19] J.D. Dent, K.J. Burrell, D.S. Schmidt, M.Y. Louge, E. Adams, T.G. Jazbutis, Density, velocity and friction measurements in a dry snow avalanche, Ann. Glaciol. 26 (1998) 247–252.
[20] M.Y. Louge, R.L. Foster, N. Jensen, R. Patterson, A portable capacitance snow sounding instrument, Cold Reg. Sci. Technol. 28 (1998) 73–81.
[21] M. Schaer, D. Issler, Particle densities, velocities and size distribution in large avalanches from impact-sensor measurements, Ann. Glaciol. 32 (2001) 321–327.

[22] B. Sovilla, M. Schaer, L. Rammer, Measurements and analysis of full-scale avalanche impact pressure at the Vallée de la Sionne test site, Cold Reg. Sci. Technol. 51 (2008) 122–137, http://dx.doi.org/10.1016/j.coldregions.2007.05.006.
[23] M.A. Kern, P. Bartelt, B. Sovilla, O. Buser, Measured shear rates in large dry and wet snow avalanches, J. Glaciol. 55 (190) (2009) 327–338.
[24] M.Y. Louge, R. Steiner, S. Keast, R. Decker, J. Dent, M. Schneebeli, Application of capacitance instrumentation to the measurement of density and velocity of flowing snow, Cold Reg. Sci. Technol. 25 (1) (1997) 47–63.
[25] B. Turnbull, J.N. McElwaine, Experiments on the non-Boussinesq flow of self-igniting suspension currents on a steep open slope, J. Geophys. Res. 113 (2008) F01003, http://dx.doi.org/10.1029/2007JF000753.
[26] K. Nishimura, F. Sandersen, K. Kristensen, K. Lied, Measurements of powder snow avalanche – nature, Surv. Geophys. 16 (1995) 649–660.
[27] L. Rammer, H. Schaffhauser, P. Sampl, Computed powder avalanche impact pressures on a tunnel-bridge in Ausserfern – Tirol, in: K. Sassa (Ed.), Environmental Forest Science. Proceedings of the IUFRO Division 8 Conference, Kluwer, Dordrecht, The Netherlands, 1998, pp. 599–605.
[28] C. Carroll, M.Y. Louge, B. Turnbull, Frontal dynamics of powder snow avalanches, J. Geophys. Res., Earth Surf. 118 (2013) 913–924.
[29] M.Y. Louge, C.S. Carroll, B. Turnbull, Role of pore pressure gradients in sustaining frontal particle entrainment in eruption currents: the case of powder snow avalanches, J. Geophys. Res. 116 (F4) (2011) F04030.
[30] F. Naaim-Bouvet, M. Naaim, M. Bacher, L. Heiligenstein, Physical modelling of the interaction between powder avalanches and defence structures, Nat. Hazards Earth Syst. Sci. 2 (2002) 193–202, http://dx.doi.org/10.5194/nhess-2-193-2002.
[31] M. Primus, F. Naaim-Bouvet, M. Naaim, T. Faug, Physical modeling of the interaction between mounds or deflecting dams and powder snow avalanches, Cold Reg. Sci. Technol. 39 (2004) 257–267, http://dx.doi.org/10.1016/j.coldregions.2004.05.006.
[32] P. Bartelt, B.W. McArdell, Granulometric investigations of snow avalanches, J. Glaciol. 55 (193) (2009) 829–833.
[33] J. Gray, Particle size segregation in granular avalanches: a brief review of recent progress, in: J. Goddard, J.T. Jenkins, P. Giovine (Eds.), AIP Conference Proceedings of IUTAM-ISIMM Symposium on Mathematical Modeling and Physical Instances of Granular Flows, vol. 1227, 2010, pp. 343–362.
[34] P. Gauer, D. Issler, Possible erosion mechanisms in snow avalanches, Ann. Glaciol. 38 (2004) 384–392.
[35] W. Steinkogler, B. Sovilla, M. Lehning, Influence of snow cover properties on avalanche dynamics, Cold Reg. Sci. Technol. 97 (2014) 121–131.
[36] D. Szabo, M. Schneebeli, Subsecond sintering of ice, Appl. Phys. Lett. 90 (15) (2007) 151916, http://dx.doi.org/10.1063/1.2721391.
[37] C.S. Carroll, B. Turnbull, M.Y. Louge, Role of fluid density in shaping eruption currents driven by frontal particle blow-out, Phys. Fluids 24 (2012) 066603.
[38] M.Y. Louge, The surprising relevance of a continuum description to granular clusters, J. Fluid Mech. 742 (2014) 1–4.
[39] F. Tiefenbacher, M.A. Kern, Experimental devices to determine snow avalanche basal friction and velocity profiles, Cold Reg. Sci. Technol. 38 (1) (2004) 17–30.
[40] J.N. McElwaine, F. Tiefenbacher, Calculating internal avalanche velocities from correlation with error analysis, Surv. Geophys. 24 (5–6) (2003) 499–524, http://dx.doi.org/10.1023/B:GEOP.0000006079.89478.04.
[41] B. Turnbull, J.N. McElwaine, C.J. Ancey, The Kulikovskiy–Sveshnikova–Beghin model of powder snow avalanches: development and application, J. Geophys. Res. 112 (2007) F0100, http://dx.doi.org/10.1029/2006JF000489.
[42] P. Beghin, X. Olagne, Experimental and theoretical study of the dynamics of powder snow avalanches, Cold Reg. Sci. Technol. 19 (1991) 317–326.
[43] C. Ancey, Powder-snow avalanches: approximation as non-Boussinesq clouds with a Richardson number-dependent entrainment function, J. Geophys. Res. 109 (2004) 1–14.
[44] B. Sovilla, J.N. McElwaine, M. Schaer, J. Vallet, Variation of deposition depth with slope angle in snow avalanches: measurements from Vallée de la Sionne, J. Geophys. Res. 115 (2010) F02016, http://dx.doi.org/10.1029/2009JF001390.
[45] J. Vallet, B. Turnbull, S. Joly, F. Dufour, Observations on powder snow avalanches using videogrammetry, Cold Reg. Sci. Technol. 39 (2004) 153–159.
[46] B. Turnbull, J.N. McElwaine, A comparison of powder-snow avalanches at Vallée de la Sionne, Switzerland, with plume theories, J. Glaciol. 53 (2007) 30–40.
[47] M.Y. Louge, B. Turnbull, C.S. Carroll, Volume growth of a powder snow avalanche, Ann. Glaciol. 53 (2012) 57–60.
[48] T.B. Benjamin, Gravity currents and related phenomena, J. Fluid Mech. 31 (1968) 209–248.
[49] J.E. Simpson, R.E. Britter, The dynamics of the head of a gravity current advancing over a horizontal surface, J. Fluid Mech. 94 (1978) 447–495.
[50] J.E. Simpson, Gravity Currents in the Environment and the Laboratory, Cambridge University Press, Cambridge, UK, 1997.
[51] F. Blanchette, M. Strauss, E. Meiburg, B. Kneller, M.E. Glinsky, High-resolution numerical simulations of resuspending gravity currents: conditions for self-sustainment, J. Geophys. Res. 110 (2005) C12022.
[52] P. Bebi, D. Kulakowski, C. Rixen, Snow avalanche disturbances in forest ecosystems—state of research and implications for management, For. Ecol. Manag. 257 (2009) 1883–1892.